Acta Mechanica 188, 209–225 (2007)
DOI 10.1007/s00707-006-0351-6
Printed in The Netherlands

Acta Mechanica

Gravity-driven film flow down an inclined wall with three-dimensional corrugations

H. Luo and **C. Pozrikidis**, La Jolla, California

Received February 27, 2006
Published online: July 4, 2006

Summary. The gravity-driven flow of a liquid film down an inclined wall with three-dimensional doubly periodic corrugations is investigated in the limit of vanishing Reynolds number. The film surface may exhibit constant or variable surface tension due to an insoluble surfactant. A perturbation analysis for small-amplitude corrugations is performed, wherein the wall geometry is expressed as a Fourier series consisting of a linear superposition of two-dimensional oblique waves defined by two base vectors. Each of the constituent perturbation flows over the individual oblique waves is further decomposed into a two-dimensional flow transverse to the oblique waves and a unidirectional flow parallel to the waves. Both the transverse and the parallel flow are calculated by carrying out an analysis in oblique coordinates, similar to that conducted for two-dimensional flow. The particular cases of flow down a wall with oblique two-dimensional, orthogonal three-dimensional, and hexagonal three-dimensional corrugations are considered. The results illustrate the surface velocity field and the distribution of the surfactant. The three-dimensional wall geometry is found to reduce the surface deformation with respect to its two-dimensional counterpart by increasing the effective wave numbers and decreasing the effective capillary number encapsulating the effect of surface tension.

1 Introduction

The gravity-driven flow of a liquid film down an inclined wall with two-dimensional (cylindrical) periodic corrugations has been the subject of numerous theoretical and experimental investigations. The main goals have been to describe the kinematic structure of the flow and quantify the relation between the volumetric flow rate and the mean film thickness [13], [25], [21], [23], [32], to assess the effect of the wall geometry on the deformation and stability of the free surface [11], [22], [24], to illustrate the effect of flow inertia [5], to investigate the effect of a soluble or insoluble surfactant [3], [15], to describe the flow of multi-layered arrangements [8], [16], and to document the effect on simultaneous heat and mass transport [12]. In recent years, Aksel and coworkers presented a series of insightful theoretical and laboratory investigations addressing various aspects of the film flow over a broad range of Reynolds numbers and wall amplitudes [20], [18], [30], [31], [19], [27], [28].

Theoretical studies of film flow based on perturbation expansions have addressed asymptotic limits where the amplitude of the corrugations is small compared to either the mean film thickness or the wave length of the corrugations. In most of these studies, the Reynolds number is assumed to be suitably small and the analysis is conducted under the auspices of Stokes or

lubrication flow. In other studies, integral momentum balances are employed to capture the dominant effect of flow inertia at high Reynolds numbers. Numerical methods for free-surface flows have been developed to describe the unknown shape of the film surface using boundary and domain discretization methods [10], [16].

Several authors have considered film flow over three-dimensional obstacles, protrusions and trenches representing a localized topography. The analysis is conducted by asymptotic methods for small-size irregularities, or else working under the auspices of the lubrication approximation [2], [4], [6], [7], [17]. By contrast, the film flow down a wall with three-dimensional (non-cylindrical) corrugations has received limited attention. Though tackling the general three-dimensional problem by numerical methods is a formidable task typical of that encountered in the computation of three-dimensional free-surface flows, a perturbation analysis for small-amplitude corrugations is amenable to standard techniques when the effect of fluid inertia is suitably small. The first effort in this direction was made recently by Wang [26] who considered film flow down an inclined wall with rectangular periodic corrugations on a bumpy substrate. His results illustrated the effect of the aspect ratio on the flow rate for a given mean film thickness.

Our main goal in this paper is to demonstrate that, in the context of Stokes flow, the computation of film flow down a wall with small-amplitude three-dimensional periodic corrugations defined by a Bravais lattice can be reconstructed in terms of a straightforward analysis for two-dimensional (transverse) and one-dimensional (longitudinal) flow down a wavy wall. The key idea is to expand the wall geometry in a Fourier series representing oblique two-dimensional waves, and then synthesize the results by linear superposition. The problem is formulated in Sect. 2, specific wall geometries are discussed in Sects. 3–5, and general remarks are made in Sect. 6.

2 Problem statement

We consider the steady flow of a liquid film down an inclined wall with three-dimensional doubly periodic corrugations in the presence of an insoluble surfactant, as illustrated in Fig. 1. In the inclined system of coordinates depicted in this figure, the base plane of the wall in the

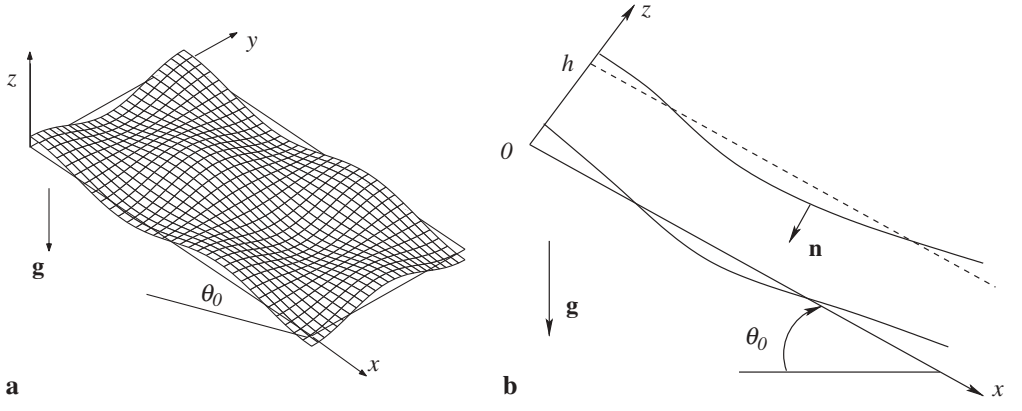

Fig. 1. Schematic illustration of film flow down an inclined plane with three-dimensional periodic corrugations. **a** Oblique view of the wall, and **b** side view of the wall and film surface

absence of corrugations is located at $z = 0$ and is inclined at an angle θ_0 with respect to the horizontal plane. The y axis lies in a horizontal plane that is normal to the acceleration of gravity vector whose Cartesian components are

$$\mathbf{g} = g\Big(\sin\theta_0,\ 0,\ -\cos\theta_0\Big), \tag{1}$$

where $g = |\mathbf{g}|$ is the magnitude of the acceleration of gravity. The geometry of the corrugated wall is described by the function

$$z = z_w(x, y). \tag{2}$$

The periodicity of the corrugations is determined by two base vectors, $\mathbf{l}_1$ and $\mathbf{l}_2$, that are parallel to the xy-plane and are defined such that

$$z_w(\mathbf{w}) = z_w(\mathbf{w} + i\ \mathbf{l}_1 + j\ \mathbf{l}_2), \tag{3}$$

where $\mathbf{w} = (x, y)$, and i and j are two integers. Note that $\mathbf{l}_1$ and $\mathbf{l}_2$ are not necessarily orthogonal; if they are, the wall corrugations form a square or, more generally, a rectangular lattice. The wall function $z_w(x, y)$ can be expanded in a two-dimensional Fourier series,

$$z_w(x, y) = \sum_{n=-\infty}^{\infty} \sum_{m=-\infty}^{\infty} c_{nm} \exp\Big(\mathrm{i}(n\mathbf{k}_1 + m\mathbf{k}_2\ ) \cdot \mathbf{w}\Big), \tag{4}$$

where c_{nm} are complex expansion coefficients, i is the imaginary unit, and $\mathbf{k}_1$, $\mathbf{k}_2$ are the reciprocal wavelength vectors satisfying

$$\mathbf{k}_i \cdot \mathbf{l}_j = 2\pi\ \delta_{ij}, \tag{5}$$

where δ_{ij} is Kronecker's delta. These properties ensure the satisfaction of the periodicity condition (3). A two-dimensional wall geometry consisting of streamwise, spanwise, or oblique corrugations arises for specific choices of the expansion coefficients, c_{nm}, one of them being $c_{nm} = 0$ for any non-zero value of m.

The Reynolds number of the flow defined with respect to the mean film thickness is assumed to be so small that the motion of the fluid is governed by the linear equations of Stokes flow including the Stokes equation and the continuity equation,

$$-\nabla p + \mu\nabla^2\mathbf{u} + \rho\mathbf{g} = \mathbf{0}, \quad \nabla \cdot \mathbf{u} = 0, \tag{6}$$

where μ and ρ are the liquid viscosity and density, $\mathbf{u} = (u, v, w)$ is the velocity, and p is the pressure. The velocity is required to satisfy the no-slip and no-penetration boundary conditions over the wall, $\mathbf{u} = \mathbf{0}$, and the hydrodynamic traction $\mathbf{f}$ is required to satisfy the dynamic boundary condition

$$\mathbf{f} = \boldsymbol{\sigma} \cdot \mathbf{n} = (2\gamma\kappa - p_a)\mathbf{n} - \nabla_s\gamma, \tag{7}$$

over the film surface, where $\boldsymbol{\sigma}$ is the Newtonian stress tensor, γ is the position-dependent surface tension, $\mathbf{n}$ is the unit normal vector pointing into the film, $\nabla_s \equiv (\mathbf{I} - \mathbf{nn}) \cdot \nabla$ is the surface gradient operator, $\kappa \equiv (1/2)\nabla_s \cdot \mathbf{n}$ is the mean curvature of the free surface, and p_a is the ambient pressure.

The surface tension, γ, is a function of the surfactant concentration, Γ, whose evolution is governed by the surface transport equation

$$\frac{d\Gamma}{dt} + \nabla_s \cdot (\Gamma\mathbf{u}_s) + 2\kappa u_n\Gamma = D_s\nabla_s^2\Gamma, \tag{8}$$

where $\mathbf{u}_s$ is the tangential velocity, $u_n = \mathbf{u} \cdot \mathbf{n}$ is the normal velocity at the film surface, and D_s is the surfactant diffusivity [14]. The derivative d/dt on the left-hand side of (8) expresses the

rate of change of a variable following the motion of interfacial marker points moving with the component of the fluid velocity normal to the film surface alone. In the case of steady flow, the first and third terms on the left-hand side of Eq. (8) vanish, yielding

$$\nabla_s \cdot (\Gamma \mathbf{u}_s) = D_s \nabla_s^2 \Gamma, \tag{9}$$

which expresses a balance between interfacial convection and diffusion.

In the context of the small-deformation theory, a linear relationship may be assumed between the surface tension and the surfactant concentration,

$$\gamma = \gamma_0 \left(1 + Ma \left(1 - \frac{\Gamma}{\Gamma_0} \right) \right), \tag{10}$$

where Γ_0 is a reference concentration corresponding to the surface tension γ_0, and Ma is the Marangoni number expressing the sensitivity of the surface tension to the surfactant concentration, $\partial\gamma/\partial\Gamma = -Ma\,\gamma_0/\Gamma_0$ [1], [16].

To carry out a linear perturbation analysis, we consider a wall whose amplitude $|z_w|$ is small compared to the mean film thickness and the magnitude of each of the two base vectors, and describe the disturbance caused by the wall undulations by superposing the disturbance flows associated with each Fourier term in (4). Specific results are presented in the next three sections for three different wall geometries.

3 Flow over oblique undulations

In the simplest possible configuration, the wall exhibits small-amplitude sinusoidal undulations described by the real or imaginary part of the complex function

$$z_w(x, y) = \epsilon h \exp\Big(\mathrm{i}(\mathbf{k}_1 + \mathbf{k}_2) \cdot \mathbf{w} \Big), \tag{11}$$

where ϵ is a dimensionless coefficient whose magnitude is much less than unity, and h is the mean film thickness. An example is shown in Fig. 3a. If $\mathbf{k}_1 = (k_{11}, k_{12})$ and $\mathbf{k}_2 = (k_{21}, k_{22})$, then Eq. (11) can be written as

$$z_w(x, y) = \epsilon h \mathrm{e}^{\mathrm{i}(\alpha_1 x + \alpha_2 y)}, \tag{12}$$

where

$$\alpha_1 \equiv k_{11} + k_{21}, \quad \alpha_2 \equiv k_{12} + k_{22}. \tag{13}$$

Thus, the wall geometry described by (12) is a one-dimensional oblique harmonic wave whose ridges are inclined at an angle θ with respect to the x-axis, where

$$\tan\theta = -\frac{\alpha_1}{\alpha_2}, \tag{14}$$

for $\theta \in [0, \pi)$. The wave number of the oblique wave is

$$\hat{k} = \sqrt{\alpha_1^2 + \alpha_2^2}. \tag{15}$$

When $\theta = 0$ we obtain unidirectional flow along the η axis, and when $\theta = \pi/2$ we obtain two-dimensional flow in the $z\xi$-plane, as shown in Fig. 2.

The Stokes flow over the oblique wavy wall can be decomposed into a transverse flow perpendicular to the ridges, and a parallel flow along the ridges. To implement this decomposition, we introduce the oblique coordinates

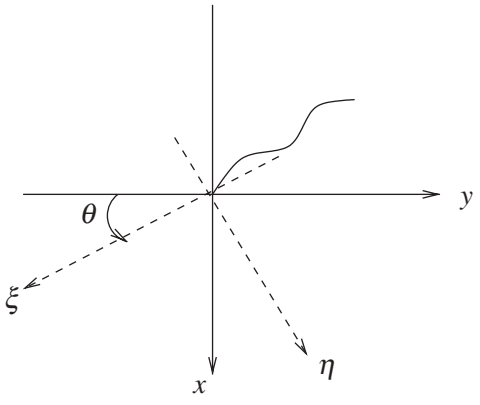

Fig. 2. Inclined coordinates used to describe flow over a wall with oblique undulations whose ridges are perpendicular to the ξ-axis

$$\xi = x\sin\theta - y\cos\theta, \quad \eta = x\cos\theta + y\sin\theta, \tag{16}$$

which are designed so that the ridges are parallel to the η axis, as shown in Fig. 2. The wall geometry stated in Eq. (12) is then described by

$$z_w(\xi) = \epsilon h \mathrm{e}^{\mathrm{i}\hat{k}\xi}. \tag{17}$$

Since the inclined coordinates (ξ, η, z) are Cartesian, transforming the governing equations of Stokes flow is straightforward. Using a caret to designate the oblique coordinates, we write the Stokes flow equations (6) as

$$-\hat{\nabla}p + \mu\hat{\nabla}^2\hat{\mathbf{u}} + \rho\hat{\mathbf{g}} = \mathbf{0}, \quad \hat{\nabla}\cdot\hat{\mathbf{u}} = 0, \tag{18}$$

where $\hat{\mathbf{u}} = (\hat{u}, \hat{v}, w)$, $\hat{\nabla} = (\partial/\partial\xi, \partial/\partial\eta, \partial/\partial z)$, and the components of the acceleration of gravity are $\hat{\mathbf{g}} = (g_\xi,\ g_\eta,\ g_z)$, with

$$g_\xi = g\sin\theta_0\sin\theta, \quad g_\eta = g\sin\theta_0\cos\theta, \quad g_z = -g\cos\theta_0. \tag{19}$$

The film surface is described by the function

$$z_s(\xi, \eta) = h + \epsilon s(\xi, \eta), \tag{20}$$

where $s(\xi, \eta)$ is the linear perturbation of the surface. The distribution of the surfactant concentration and surface tension along the film surface are described by the companion functions

$$\Gamma(\xi, \eta) = \Gamma^{(0)} + \epsilon\Gamma^{(1)}(\xi, \eta), \quad \gamma(\xi, \eta) = \gamma^{(0)} + \epsilon\gamma^{(1)}(\xi, \eta), \tag{21}$$

where $\Gamma^{(0)} = \Gamma_0$ and $\gamma^{(0)} = \gamma_0$ are uniform values corresponding to unidirectional flow. Since the perturbation is small, we may write

$$\gamma^{(1)} = -Ma\frac{\gamma_0}{\Gamma_0}\Gamma^{(1)}, \tag{22}$$

based on Eq. (10).

The velocity components, $\hat{u}$, $\hat{v}$, and w, and pressure, p, can be expanded in the perturbation series

$$(\hat{u}, \hat{v}, w, p) = \left(\hat{u}^{(0)}, \hat{v}^{(0)}, w^{(0)}, p^{(0)}\right) + \epsilon\left(\hat{u}^{(1)}, \hat{v}^{(1)}, w^{(1)}, p^{(1)}\right) + \ldots, \tag{23}$$

where the leading-order terms, corresponding to the flat-film Nusselt solution, are given by

$$\begin{aligned} &\hat{u}^{(0)} = \frac{\hat{U}}{h^2}z(2h - z), \quad \hat{v}^{(0)} = \frac{\hat{V}}{h^2}z(2h - z), \quad w^{(0)} = 0, \\ &p^{(0)} = p_a + \rho g\cos\theta_0(h - z), \end{aligned} \tag{24}$$

$\hat{U} \equiv U \sin\theta$ and $\hat{V} \equiv U \cos\theta$ are the unperturbed surface velocities in the ξ and η directions, respectively, and $U \equiv \rho g h^2 \sin\theta_0/(2\mu)$ is the unperturbed surface velocity along the x-axis. Linearizing the governing equation with respect to ϵ, we find that the first-order solution satisfies the equations of unforced Stokes flow,

$$-\hat{\nabla} p^{(1)} + \mu \hat{\nabla}^2 \hat{\mathbf{u}}^{(1)} = \mathbf{0}, \quad \hat{\nabla} \cdot \hat{\mathbf{u}}^{(1)} = 0. \tag{25}$$

Kinematic compatibility requires that $D(z_s - z)/Dt = 0$, where D/Dt is the material derivative. Linearizing at steady state, we find

$$\hat{u}^{(0)} \frac{\partial s}{\partial \xi} + \hat{v}^{(0)} \frac{\partial s}{\partial \eta} - w^{(1)} = 0, \tag{26}$$

evaluated at $z = h$. Linearizing the no-slip and no-penetration conditions at the wall, we find

$$\hat{u}^{(1)} + \frac{\partial \hat{u}^{(0)}}{\partial z} h e^{i\hat{k}\xi} = 0, \quad \hat{v}^{(1)} + \frac{\partial \hat{v}^{(0)}}{\partial z} h e^{i\hat{k}\xi} = 0, \quad w^{(1)} = 0, \tag{27}$$

evaluated at $z = 0$. The counterpart of the free-surface condition (7) in the $\xi\eta z$ coordinates indicated by the caret is $\hat{\sigma} \cdot \hat{\mathbf{n}} = (2\gamma\kappa - p_a)\hat{\mathbf{n}} - \hat{\nabla}_s \gamma$. Linearizing the mean curvature and the surface normal, we find

$$2\kappa \approx \epsilon \left(\frac{\partial^2 s}{\partial \xi^2} + \frac{\partial^2 s}{\partial \eta^2} \right), \quad \hat{\mathbf{n}} \approx \left(\epsilon \frac{\partial s}{\partial \xi}, \epsilon \frac{\partial s}{\partial \eta}, -1 \right), \tag{28}$$

yielding the linearized surface condition

$$\begin{pmatrix} \mu \left(\dfrac{\partial \hat{u}^{(1)}}{\partial z} + \dfrac{\partial w^{(1)}}{\partial \xi} \right) \\ \mu \left(\dfrac{\partial \hat{v}^{(1)}}{\partial z} + \dfrac{\partial w^{(1)}}{\partial \eta} \right) \\ -p^{(1)} + 2\mu \dfrac{\partial w^{(1)}}{\partial z} \end{pmatrix} + s \begin{pmatrix} \mu \dfrac{\partial^2 \hat{u}^{(0)}}{\partial z^2} \\ \mu \dfrac{\partial^2 \hat{v}^{(0)}}{\partial z^2} \\ -\dfrac{\partial p^{(0)}}{\partial z} \end{pmatrix} = \gamma_0 \begin{pmatrix} 0 \\ 0 \\ \dfrac{\partial^2 s}{\partial \xi^2} + \dfrac{\partial^2 s}{\partial \eta^2} \end{pmatrix} + \begin{pmatrix} \dfrac{\partial \gamma^{(1)}}{\partial \xi} \\ \dfrac{\partial \gamma^{(1)}}{\partial \eta} \\ 0 \end{pmatrix}, \tag{29}$$

where all terms are evaluated at $z = h$. To complete the formulation of the linear problem, we substitute Eq. (21) into the transport equation (9) written in the $\xi\eta z$ coordinates, and obtain

$$\hat{u}^{(0)} \frac{\partial \Gamma^{(1)}}{\partial \xi} + \hat{v}^{(0)} \frac{\partial \Gamma^{(1)}}{\partial \eta} - \Gamma_0 \frac{\partial w^{(1)}}{\partial z} = D_s \left(\frac{\partial^2 \Gamma^{(1)}}{\partial \xi^2} + \frac{\partial^2 \Gamma^{(1)}}{\partial \eta^2} \right), \tag{30}$$

where all the terms are evaluated at $z = h$.

Equations (22), (25)–(27), (29) and (30) constitute a set of linear differential equations. Stipulating that all variables are independent of η, we set the η derivatives equal to zero, and find that the η velocity component, $\hat{v}$, does not affect the rest of unknowns, including the surfactant concentration $\Gamma^{(1)}$ and surface position s. Physically, the flow can be decoupled into a two-dimensional flow in the ξz-plane, and a unidirectional parallel cross flow in the ηz-plane. The two-dimensional flow determines the shape of the interface and distribution of the surfactant, and is not affected by the cross flow. On the other hand, the cross flow is affected by the two-dimensional flow through the deformed shape of the shape, as can be seen in the second equation in (29).

The solution of the two-dimensional flow can be found using a standard method [25], [15]. To begin, we express the first-order perturbations as

$$\begin{aligned} &s = Ah\mathrm{e}^{\mathrm{i}\hat{k}\xi}, \quad \Gamma^{(1)} = C\Gamma_0\mathrm{e}^{\mathrm{i}\hat{k}\xi}, \quad \gamma^{(1)} = D\gamma_0\mathrm{e}^{\mathrm{i}\hat{k}\xi}, \\ &\hat{u}^{(1)} = \hat{U}f'(\check{z})\mathrm{e}^{\mathrm{i}\hat{k}\xi}, \quad w^{(1)} = -\mathrm{i}\hat{k}\hat{U}hf(\check{z})\mathrm{e}^{\mathrm{i}\hat{k}\xi}, \end{aligned} \tag{31}$$

where

$$f(\check{z}) = a_1\mathrm{e}^{\check{k}\check{z}} + a_2\check{z}\mathrm{e}^{\check{k}\check{z}} + a_3\mathrm{e}^{-\check{k}\check{z}} + a_4\check{z}\mathrm{e}^{-\check{k}\check{z}}, \tag{32}$$

A, C, D, a_i, $i = 1, \ldots, 4$ are dimensionless complex coefficients, $\check{k} = \hat{k}h$, and $\check{z} = z/h$. The unknown coefficients are obtained by solving the linear algebraic system

$$\mathbf{M} \cdot \mathbf{z} = \mathbf{q}, \tag{33}$$

where $\mathbf{z} = [a_1, a_2, a_4, D]^T$ and $\mathbf{q} = [-2, 0, 0, 0]^T$, complemented by $D = -MaC$, $A = -f(1)$, and $a_3 = -a_1$. The matrix $\mathbf{M}$ is given by

$$\mathbf{M} = \begin{bmatrix} 2\check{k} & 1 & 1 & 0 \\ (1-q)(\check{k}^2+1) & \check{k}^2+\check{k}+1 & q(\check{k}^2-\check{k}+1) & -\dfrac{2\pi^2\mathrm{i}}{Ca_\xi\check{k}}\mathrm{e}^{-\check{k}} \\ \check{k}^2(1+q)-\mathrm{i}\tau(1-q) & \check{k}^2-\mathrm{i}\tau & -q(\check{k}^2+\mathrm{i}\tau) & 0 \\ Ma\check{k}(1+q) & Ma(1+\check{k}) & Maq(1-\check{k}) & -\left(1-\dfrac{2\pi\mathrm{i}}{Pe}\right)\mathrm{e}^{-\check{k}} \end{bmatrix}, \tag{34}$$

where $q \equiv \exp(-2\check{k})$,

$$\tau \equiv \cot\theta_0/\sin\theta + 2\pi^2/Ca_\xi, \tag{35}$$

and

$$Ca_\xi \equiv (\mu\hat{U}/\gamma_0)(\hat{l}/h)^2 \tag{36}$$

is the effective capillary number, $\hat{l} = 2\pi/\hat{k}$ is the effective wavelength, and $Pe = \hat{l}\hat{U}/D_s$ is the surfactant surface Péclet number. The effective capillary number Ca_ξ expresses the magnitude of viscous stresses, $\mu\hat{U}/h$, relative to the capillary pressure, $h\gamma_0/\hat{l}^2$. In the absence of surfactant, $Ma = 0$, only the northwestern 3×3 portion of the matrix $\mathbf{M}$ is relevant.

To solve for the cross flow, we set $\hat{v}^{(1)} = \hat{V}r(\check{z})\mathrm{e}^{\mathrm{i}\hat{k}\xi}$, and substitute in Eq. (25) to obtain

$$r'' - \check{k}^2 r = 0. \tag{37}$$

The general solution is $r(\check{z}) = b_1\mathrm{e}^{\check{k}\check{z}} + b_2\mathrm{e}^{-\check{k}\check{z}}$, where b_1 and b_2 are dimensionless coefficients. The no-slip boundary condition at the lower wall shown in (27) and the dynamic condition at the surface shown in (29) require, respectively, $r(\check{z}=0) = -2$ and $r'(\check{z}=1) = -2A$. Using these conditions, we find that b_1 and b_2 are given by

$$b_1 = \frac{-\mathrm{e}^{-\check{k}} + A/\check{k}}{\cosh\check{k}}, \quad b_2 = -\frac{\mathrm{e}^{\check{k}} + A/\check{k}}{\cosh\check{k}}. \tag{38}$$

The structure of the flow down the oblique wave depends on the dimensionless wave number $\check{k}$, plane inclination angle θ_0, obliqueness angle θ, capillary number Ca_ξ, Marangoni number Ma, and Pe determining the surfactant diffusivity.

As an example, Fig. 3a, b, c shows the wall profile, the film surface, and the surface velocity field in the absence of surfactants, $Ma = 0$, for $\theta_0 = \pi/4$, $Ca \equiv \mu U/\gamma_0 = \sqrt{2}/4$, $\alpha_1 h = 1$, and $\alpha_2 h = -\sqrt{3}/3$. The dimensionless oblique wave number in this case is $\hat{k}h = 2\sqrt{3}/3$, and the

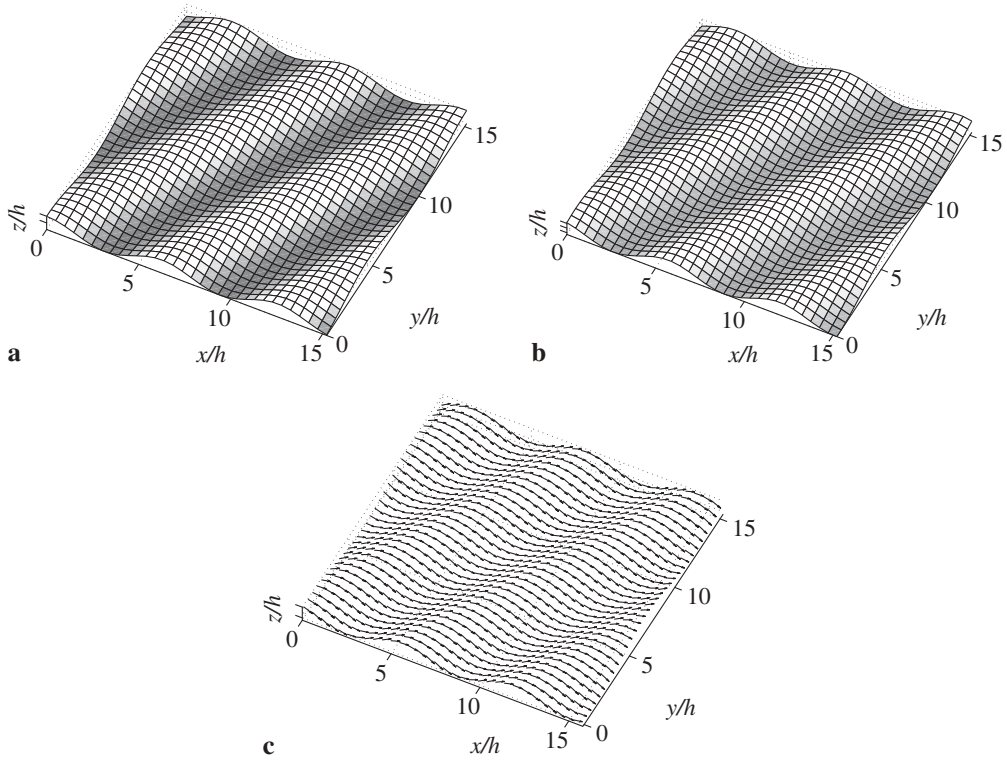

Fig. 3. Flow down a wavy wall with oblique sinusoidal undulations described by $z_w = \epsilon h \cos(\alpha_1 x + \alpha_2 y)$. **a** Wall geometry for $\alpha_1 h = 1$ and $\alpha_2 h = -\sqrt{3}/3$, **b** film surface, and **c** velocity vector field for $Ca \equiv \mu U/\gamma_0 = \sqrt{2}/4$, $\theta_0 = \pi/4$, and $Ma = 0$

effective capillary number is $Ca_\xi = (3\sqrt{6}/8)\pi^2$. Linear analysis predicts that the dimensionless amplitude of the surface is $|A| = 0.5511$ and the phase shift is $\arg(A) = 0.1771\pi$. Figure 3b shows that the surface wave is parallel to the wall corrugations, but is shifted upstream perpendicular to the oblique ridges. The surface velocity vector field depicted in Fig. 3c indicates that, although the fluid velocity follows the wavy surface, it turns slightly in the y direction at the upstream side of the wave crest, and in the $-y$ direction at the downstream side of the corrugations.

4 Flow over a wall with three-dimensional orthogonal corrugations

In the next case study, we consider flow down a genuinely three-dimensional wall described by the shape function

$$z_w = \epsilon h \cos(k_1 x)\cos(k_2 y), \tag{39}$$

where k_1 and k_2 are the x and y wave numbers, as shown in Fig. 4. Cursory inspection reveals that this wall shape function can be reconstructed as a linear combination of the two cosine Fourier modes

$$\cos(k_1 x + k_2 y), \quad \cos(k_1 x - k_2 y), \tag{40}$$

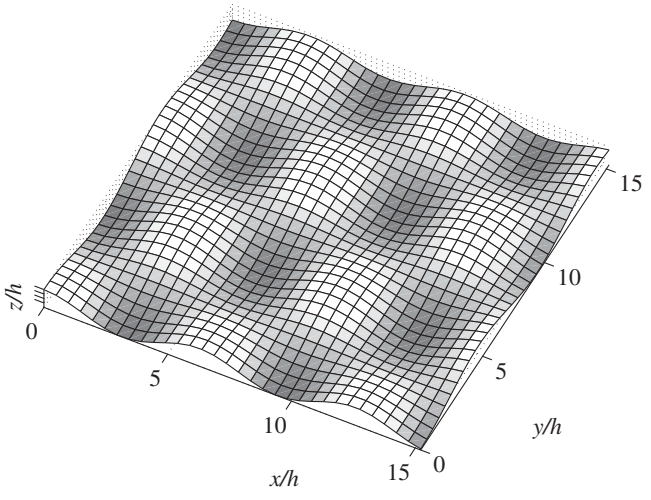

Fig. 4. Illustration of a bumpy wall with three-dimensional orthogonal corrugations described by the function $z_w = \epsilon h \cos(k_1 x)\cos(k_2 y)$

representing oblique waves that are symmetric about the x-axis, with equal oblique wave numbers, $\hat{k} = \sqrt{k_1^2 + k_2^2}$, and identical amplitudes. The surface of the deformed film is described by

$$z_s(x,y) = h + \frac{1}{2}\epsilon|A|h\big(\cos\big[\hat{k}\xi_1 + \arg(A)\big] + \cos\big[\hat{k}\xi_2 + \arg(A)\big]\big), \tag{41}$$

where

$$\xi_1 = x\sin\theta - y\cos\theta, \quad \xi_2 = x\sin(\pi-\theta) - y\cos(\pi-\theta), \tag{42}$$

$\sin\theta = k_1/\hat{k}$, $\cos\theta = -k_2/\hat{k}$, and the complex amplitude, A, is computed as discussed in Section 3 for either one of the two modes. Simplifying, we find

$$z_s(x,y) = h + \epsilon|A|h\cos[k_1 x + \arg(A)]\cos(k_2 y). \tag{43}$$

As expected on geometrical reasoning, the surface deformation is displaced with respect to the wall in the streamwise direction by an amount that is determined by $\arg(A)$.

Figure 5a, b shows the amplitude and phase shift of the film surface for $Ma = 0$, $\theta_0 = \pi/20$ and $\pi/4$, and $k_1 h = 1$, over a range of $k_2 h$. The capillary number based on the surface velocity of the unidirectional flow is $Ca \equiv \mu U/\gamma_0 = \sqrt{2}/4$. As $k_2 h$ tends to zero, the surface amplitude approaches a well defined limit. Physically, in the limit of long wave length in the y direction, the wall corrugations become two-dimensional, and the surface amplitude tends to $|A| = 0.4028$ for $\theta_0 = \pi/20$, and to $|A| = 0.6428$ for $\theta_0 = \pi/4$. On the other hand, as $k_2 h$ increases, the surface amplitude decreases monotonically to zero. Physically, the effective wave number $\hat{k}$ of the oblique waves becomes higher, and the effective capillary number Ca_ξ defined in (36) becomes lower, so that the surface deformation is reduced. As $k_2 h$ tends to zero, the phase shift of the free surface tends to $\arg(A) = 0.3063\pi$ for $\theta_0 = \pi/20$ and $\arg(A) = 0.1341\pi$ for $\theta_0 = \pi/4$. As $k_2 h$ is increased from low values, the phase shift increases monotonically toward a certain asymptotic limit.

Figure 6a shows a contour plot of the wall and the film surface for $k_2 h = 1$ and $\theta_0 = \pi/4$. The dimensionless amplitude of the free surface is $|A| = 0.4020$, and the phase-shift is $\arg(A) = 0.2466\pi$. The shape of the free surface is identical to that of the wall, except that it is somewhat shifted upstream. Figure 6b shows the shape of the free surface, and Fig. 6c shows

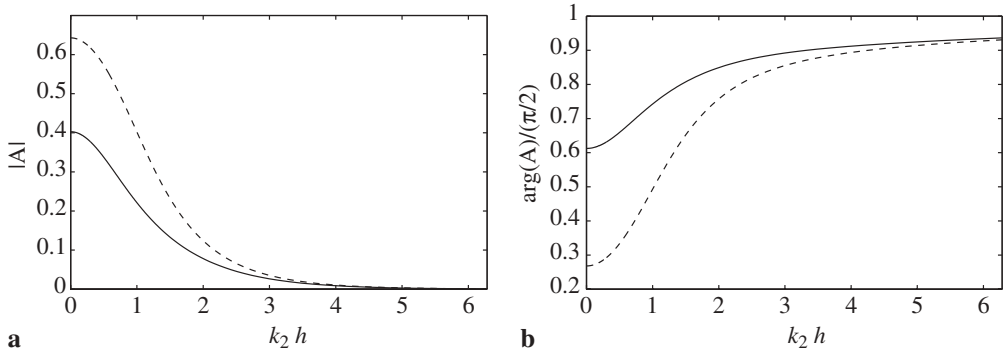

Fig. 5. Film flow over a three-dimensional wavy wall described by $z_w = \epsilon h \cos(k_1 x)\cos(k_2 y)$, for $k_1 h = 1$, $Ca = \sqrt{2}/4$, $\theta_0 = \pi/20$ (solid lines) or $\pi/4$ (dashed lines), and $Ma = 0$. **a** Surface amplitude, and **b** phase shift with respect to the wall

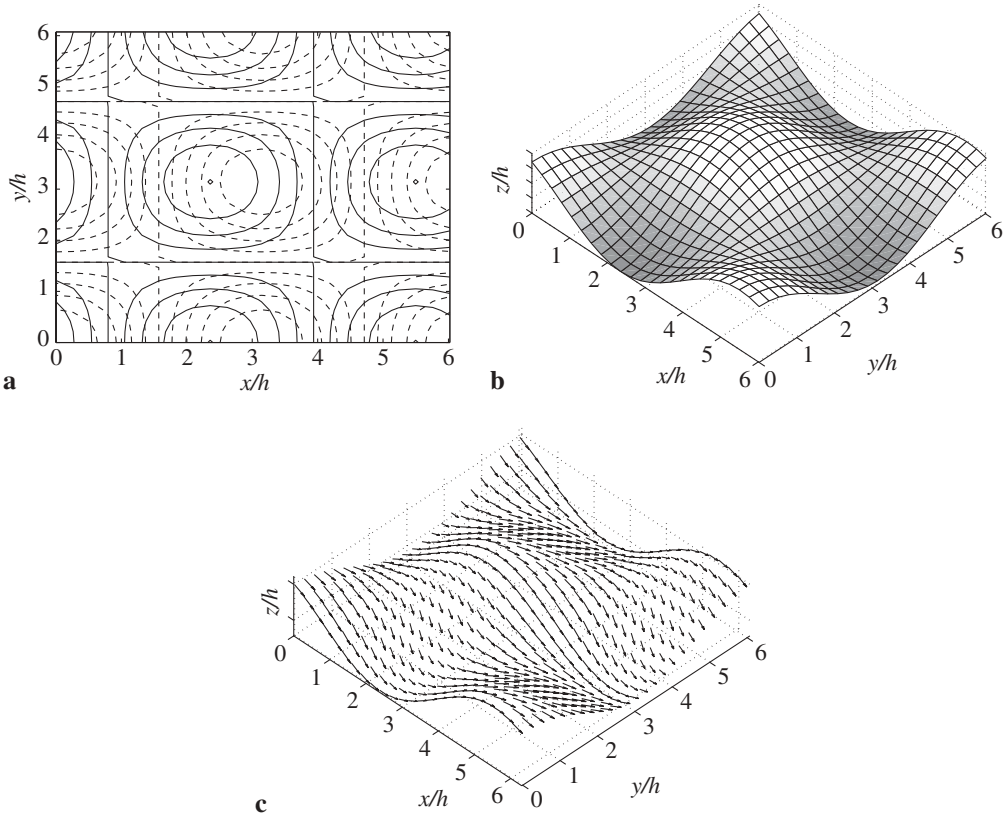

Fig. 6. **a** Contours of the free surface (solid lines) and wall topography (dashed lines) for wall geometry $z_w = \epsilon h \cos(k_1 x)\cos(k_2 y)$, $k_1 h = k_2 h = 1$, $Ca = \sqrt{2}/4$, $\theta_0 = \pi/4$, and $Ma = 0$. **b** Film surface, and **c** surface velocity vector field

the surface velocity vector field. Although the surface velocity is dominated by the mean flow along the x-axis, deviations from the unidirectional flow occur over the slopes of the bumpy surface.

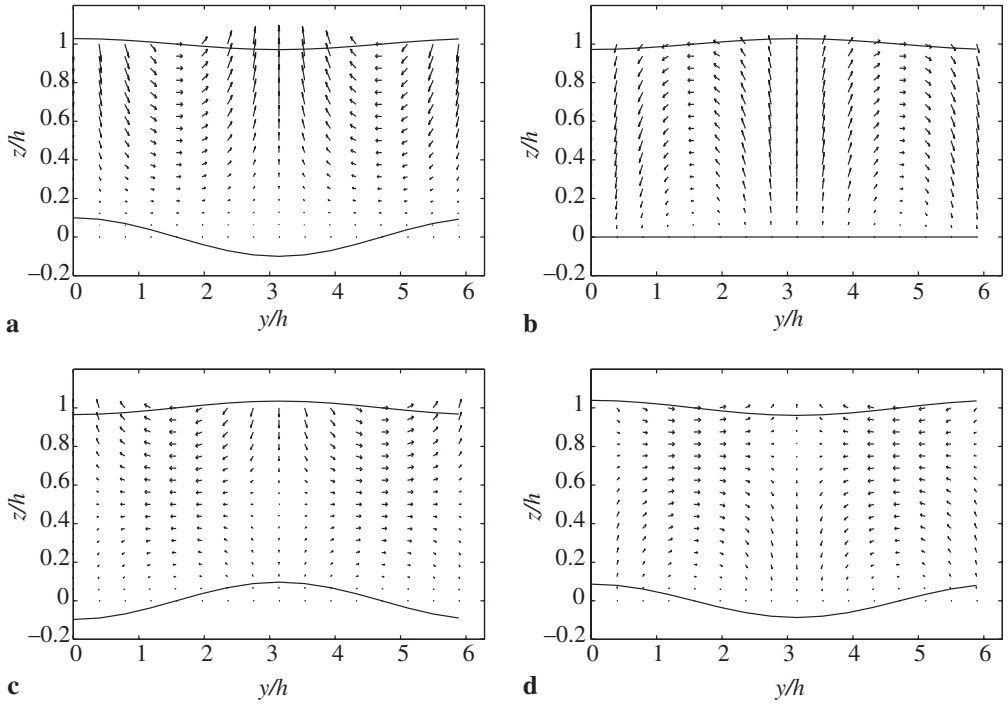

Fig. 7. Velocity perturbation field in the yz plane at **a** $x/h = 0$, **b** $x/h = 0.50\pi$, **c** $x/h = 0.92\pi$, and **d** $x/h = 1.83\pi$, for wall geometry $z_w = \epsilon h \cos(k_1 x)\cos(k_2 y)$, $k_1 h = k_2 h = 1$, $Ca = \sqrt{2}/4$, $\theta_0 = \pi/4$, and $Ma = 0$. The solid lines represent the wall profile and the film surface

Figure 7 shows the perturbation velocity field in the cross-flow plane at $x/h = 0$, 0.5π, 0.92π, and 1.83π. The magnified wall and free surface profiles are shown as solid lines. Note that the flow is symmetric about the $y/h = \pi$-plane. The onset of regions of recirculating flow at several locations in the yz-plane, centered at the surface, the wall, or both, is an important feature of the perturbation velocity field. Figure 8 shows the velocity disturbance field in the xz-plane at $y/h = 0$ and 0.75π. As in Fig. 7, the magnified wall and surface profiles are shown as solid lines. The perturbation flow field features two vortices centered at the free surface. However, it should be noted that the appearance of eddies in the perturbation flow does not imply that regions of recirculating flow will be observed when the perturbation flow is added to the unperturbed unidirectional flow for suitably small wall amplitudes.

The flow considered in this section was recently analyzed by Wang [26] in the absence of surfactants using a different approach. In Wang's method, the problem is formulated in primary variables defined with respect to the fixed system of Cartesian coordinates, (x, y, z), defined in Fig. 1. A perturbation expansion is then implemented to yield a sequence of problems governing the linear and quadratic perturbations due to the unevenness of the wall. Because the flow is genuinely three-dimensional, all three velocity components must be computed at once by solving an involved system of coupled differential equations that are derived with the aid of symbolic manipulation software. The results of Wang's linear analysis are identical to those presented in this Section for $Ma = 0$ using the Fourier decomposition.

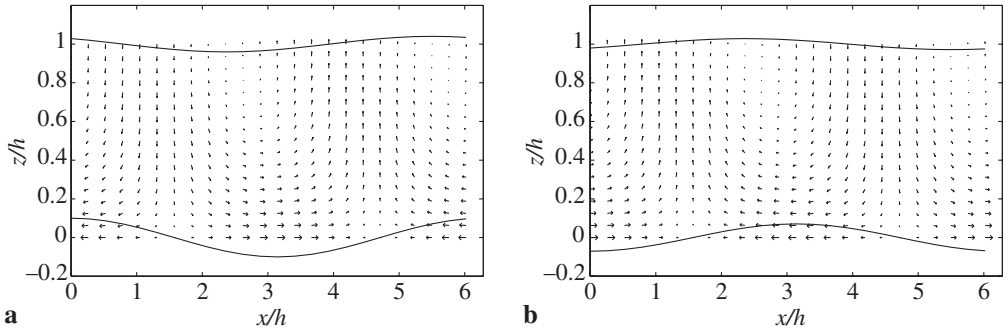

Fig. 8. Velocity perturbation field in the xz plane at locations **a** $y/h = 0$ and **b** $y/h = 0.75\pi$ for wall geometry $z_w = \epsilon h \cos(k_1 x)\cos(k_2 y)$, $k_1 h = k_2 h = 1$, $Ca = \sqrt{2}/4$, $\theta_0 = \pi/4$, and $Ma = 0$. The solid lines depict the wall profile and the film surface

5 Flow over a wall with three-dimensional non-orthogonal corrugations

In the third case study, we consider flow down a wall with non-orthogonal corrugations described by the base vectors $\mathbf{l}_1 = L(1, 0)$ and $\mathbf{l}_2 = L(-\frac{1}{2}, \frac{\sqrt{3}}{2})$, corresponding to the hexagonal lattice, where L is the lattice side length. The associated reciprocal wave number vectors are $\mathbf{k}_1 = \alpha(1, 1/\sqrt{3})$ and $\mathbf{k}_2 = \alpha(0, 2/\sqrt{3})$, where $\alpha = 2\pi/L$. The particular wall function considered is described by the equation

$$z_w = \epsilon h \cos(\mathbf{k}_1 \cdot \mathbf{x})\Big(\frac{1}{2} + \cos(\mathbf{k}_2 \cdot \mathbf{x})\Big). \tag{44}$$

A contour plot of the wall geometry is shown in Fig. 9a, where positive elevations are represented by solid lines and negative elevations are represented by dashed lines. The highest and lowest points of the wall topography form a hexagonal pattern. A three-dimensional view is shown in Fig. 9b. In this case, the wall function can be decomposed into a linear combination of three oblique waves of equal amplitude,

$$z_w = \epsilon h \, \frac{1}{2} \, (z_{w1} + z_{w2} + z_{w3}), \tag{45}$$

where

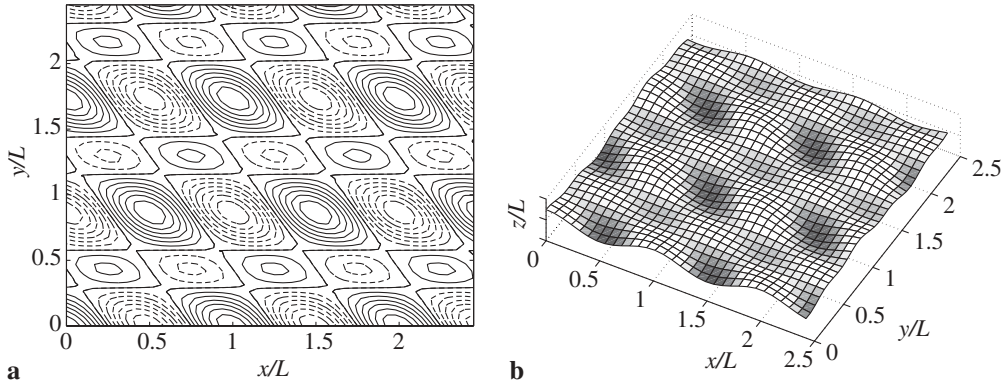

Fig. 9. **a** Contours and **b** three-dimensional view of a wall topography with a hexagonal pattern defined in the text. Positive levels are shown as solid lines, and negative levels are shown as dashed lines

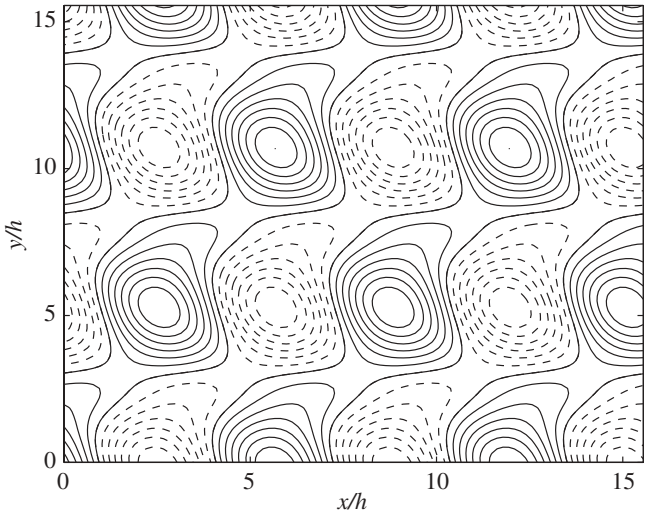

Fig. 10. Contours of the free surface for flow over wall topography with a hexagonal pattern for $\alpha h = 1$, $Ca = \sqrt{2}/4$, $\theta_0 = \pi/4$, and $Ma = 0$. Positive levels are shown as solid lines, and negative levels are shown as dashed lines

$$z_{w_1} = \cos[\alpha(x + \sqrt{3}y)], \quad z_{w_2} = \cos\left[\alpha\left(x - \frac{y}{\sqrt{3}}\right)\right], \quad z_{w_3} = \cos\left[\alpha\left(x + \frac{y}{\sqrt{3}}\right)\right]. \tag{46}$$

The wave numbers of the individual waves are $\hat{k}_1 = 2\alpha$ and $\hat{k}_2 = \hat{k}_3 = 2\alpha/\sqrt{3}$.

Figure 10 shows contours of the surface flow for $\alpha h = 1$, $Ca = \sqrt{2}/4$, $\theta_0 = \pi/4$, and $Ma = 0$. We observe that the shape of the free surface deviates significantly from that of the wall. Linear analysis predicts that the dimensionless complex amplitude of the surface associated with each constituent oblique wave is $A_1 = 0.0771 + 0.1560\mathrm{i}$, $A_2 = A_3 = 0.4680 + 0.2910\mathrm{i}$. The linear combination results in a surface with amplitude equal to 0.4254 times the maximum amplitude of the wall, $1.5\epsilon h$. As a reference point, we note that, in the case of a two-dimensional wall with the same period length in the x direction described by $z_w = \epsilon h \cos(x/h)$, the surface amplitude under the same conditions has the higher value of $|A| = 0.6428$. We conclude that three-dimensional corrugations reduce the deformation of the film with respect to the analogous two-dimensional flow.

Figure 11 illustrates the perturbation velocity field in the yz-plane at $x/h = 0$ and 0.5π, involving two regions of recirculating flow near the wall and free surface. However, the presence of these eddies does not imply that regions of recirculating flow will arise when the perturbation flow is added to the unperturbed unidirectional flow for suitably small wall amplitudes. The shape of the free surface considerably deviates from that of the wall, exhibiting a slight phase shift along the y-axis. Figure 12 illustrates the film surface, velocity vector field, and velocity disturbances over the surface. As in Fig. 6a, the fluid velocity deviates from the xz-plane and points slightly to the surface troughs due to the three-dimensionality of the flow. The disturbance field shows that the induced flow is driven away from the surface humps into the valleys.

Next, we consider film flow in the presence of a surfactant. Figure 13a shows contours of the free surface for flow over the hexagonal pattern described by Eq. (44), for $\alpha h = 1$, $Ca = \sqrt{2}/4$, $\theta_0 = \pi/4$, $Ma = 3$, and $D_s = 0$. Although the shape of the contaminated surface is generally similar to that of the clean surface shown in Fig. 10, slight differences in the phase can be observed along the x- and y-axes. Linear analysis predicts that the dimensionless complex amplitude of the surface for each individual oblique wave is

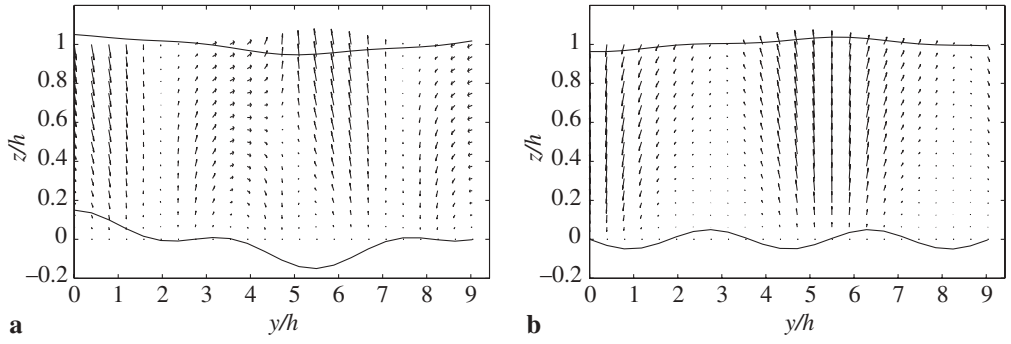

Fig. 11. Perturbation velocity field in the yz plane at **a** $x/h = 0$, and **b** $x/h = 0.5\pi$ for $Ca = \sqrt{2}/4$, $\theta_0 = \pi/4$, and $Ma = 0$

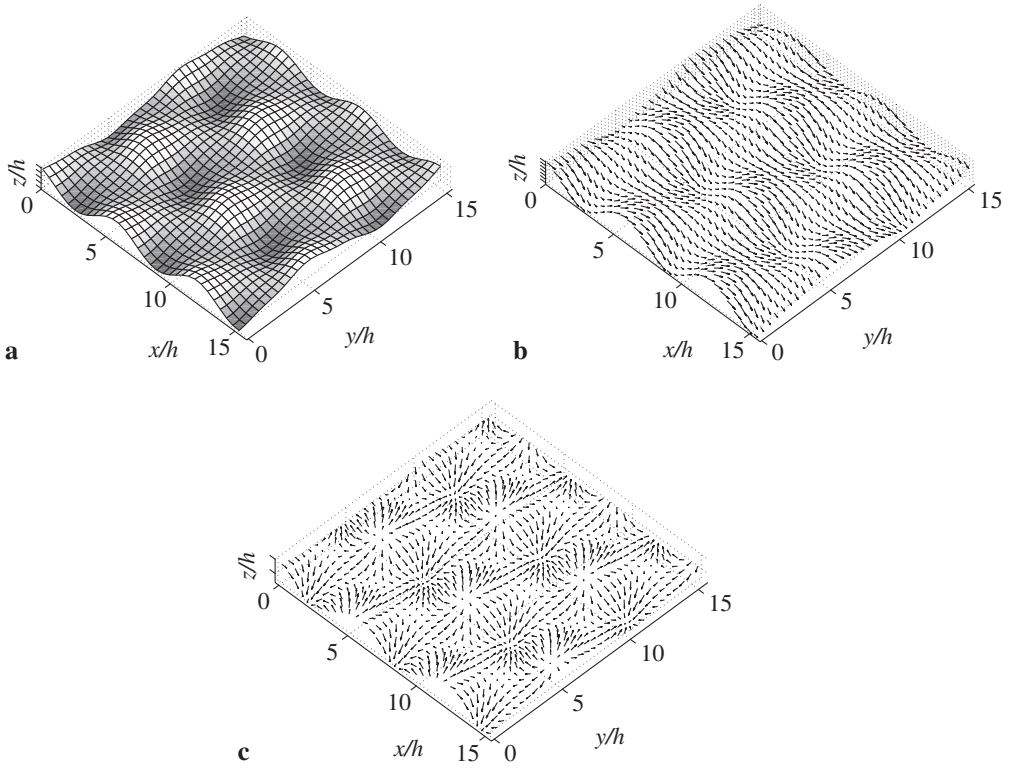

Fig. 12. **a** Film surface, **b** surface velocity field, and **c** disturbance surface velocity field for $\alpha h = 1$, $Ca = \sqrt{2}/4$, $\theta_0 = \pi/4$, and $Ma = 0$

$A_1 = 0.1010 + 0.1848\mathrm{i}$ and $A_2 = A_3 = 0.6196 + 0.2609\mathrm{i}$. The linear combination results in a free surface amplitude that is 0.5184 times the maximum amplitude of the wall, $1.5\epsilon h$. It is worth noting that the surfactant acts to increase the amplitude of the surface with respect to that of a clean surface. Figure 13b shows a contour plot of the surfactant concentration field. Comparing the two panels in Fig. 13 shows that, in this case, the surfactant field is shifted by an amount that is almost equal to π in the x direction with respect to the free surface.

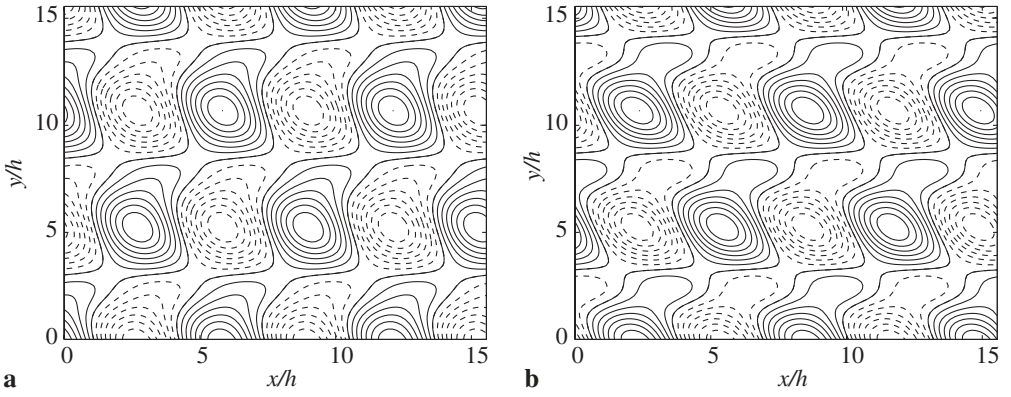

Fig. 13. **a** Film surface contours for $\alpha h = 1$, $Ca = \sqrt{2}/4$, $\theta_0 = \pi/4$, $Ma = 3$, and $D_s = 0$. **b** Contours of the surfactant concentration over the surface. Positive levels are shown as solid lines, and negative levels are shown as dashed lines

6 Discussion

We have studied the effect of small-amplitude three-dimensional wall corrugations on the gravity-driven film flow using a perturbation analysis for Stokes flow. The film surface is occupied by an insoluble surfactant that alters the local surface tension according to a linear equation of state. The amplitudes of the wall undulations are restricted to be small compared to the film thickness and wavelength, so that linearization around the flat shape can be applied. In the linear analysis, the equation describing the geometry of a wall with doubly periodic corrugations was expanded in a Fourier series consisting of oblique waves, and the flow over each oblique wave was further decomposed into a two-dimensional flow transverse to the ridges and a unidirectional flow parallel to the ridges. The shape of the free surface over each oblique wave is independent of the parallel flow and is determined by the transverse flow alone according to a linear analysis for two-dimensional flow. On the other hand, the parallel flow is affected by the transverse flow through the dynamic condition at the deformed free surface. The perturbation analysis was applied for three wall geometries. The results showed that three-dimensional corrugations reduce the surface deformation by increasing the effective wave numbers and reducing the effective capillary, compared to their two-dimensional counterparts. As in the case of two-dimensional flow, introducing surfactant amplifies the film deformation.

A natural extension of the present analysis considers the effect of fluid inertia for flow at non-zero Reynolds numbers governed by the Navier-Stokes equation. As in the case of Stokes flow, Fourier decomposition can be applied, and the flow over each oblique wave can be decomposed into a two-dimensional transverse flow and a one-dimensional flow parallel to the oblique corrugations. However, at finite Reynolds numbers, the analytical Stokes flow solution for the transverse flow employed in this work must be replaced by a numerical solution of the Navier-Stokes equation. While the transverse flow is independent of the parallel flow, the converse is not true because of both the nonlinear interaction of the perturbation transverse flow with the zeroth-order parallel flow in the convective term of the equation of motion, and the displaced position of the free surface. In future work, numerical methods will be developed to study the three-dimensional inertial film flows.

Acknowledgements

This research was supported by a grant provided by the National Science Foundation.

References

[1] Adamson, A. W.: Physical chemistry of surfaces. London: Wiley 1990.
[2] Bielarz, C., Kalliadasis, S.: Time-dependent free-surface thin film flows over topography. Phys. Fluids **15**, 2512–2524 (2003).
[3] Blyth, M. G., Pozrikidis, C.: Effect of surfactant on the stability of film flow down an inclined plane. J. Fluid Mech. **521**, 241–250 (2005).
[4] Blyth, M. G., Pozrikidis, C.: Film flow down an inclined plane over a three-dimensional obstacle. Phys. Fluids, in print (2006).
[5] Bontozoglou, V., Papapolymerou, G.: Laminar flow down a wavy incline. Int. J. Multiphase Flow **23**, 69–97 (1997).
[6] Decré M. M. J., Baret, J.-C.: Gravity-driven flows of viscous liquids over two-dimensional topographies. J. Fluid Mech. **487**, 147–166 (2003).
[7] Gaskell, P. H., Jimack, P. K., Sellier, M., Thompson, H. M. Wilson, M. C. T.: Gravity-driven flow of continuous thin liquid films on non-porous substrates with topography. J. Fluid Mech. **509**, 253–280 (2004).
[8] Kang, F., Chen, K.: Gravity-driven two-layer flow down a slightly wavy periodic incline at low Reynolds numbers. Int. J. Multiphase Flow **21**, 501–513 (1995).
[9] Li, X., Pozrikidis, C.: The effect of surfactants on drop deformation and on the rheology of dilute emulsions in Stokes flow. J. Fluid Mech. **341**, 165–194 (1997).
[10] Malamataris, N. A., Bontozoglou, V.: Computer aided analysis of viscous film flow along an inclined wavy wall. J. Comp. Phys. **154**, 372–392 (1999).
[11] Mazouchi, A., Homsy, G. M.: Free surface Stokes flow over topography. Phys. Fluids **13**, 2751–2761 (2001).
[12] Negny, S., Meyer, M., Prevost, M.: Study of laminar falling film flowing over a wavy wall column: Part I. Numerical investigation of the flow pattern and the coupled heat and mass transfer. Int. J. Heat Mass Transf. **44**, 2137–2146 (2001).
[13] Pozrikidis, C.: The flow of a liquid film along a periodic wall. J. Fluid Mech. **188**, 275–300 (1988).
[14] Pozrikidis, C.: Interfacial dynamics for Stokes flow. J. Comp. Phys. **169**, 250–301 (2001).
[15] Pozrikidis, C.: Effect of surfactants on film flow down a periodic wall. J. Fluid Mech. **496**, 105–127 (2003).
[16] Pozrikidis, C.: Instability of multi-layer channel and film flows. Adv. Appl. Mech. **40**, 179–239 (2004).
[17] Pozrikidis, C., Thoroddsen, S. T.: The deformation of a liquid film flowing down an inclined plane wall over a small particle arrested on the wall. Phys. Fluids **3**, 2546–2558 (1991).
[18] Scholle, M., Wierschem, A., Aksel, N.: Creeping film flow down an inclined wavy plane. Part I. ZAMM **81**, S487-S488 (2001).
[19] Scholle, M., Wierschem, A., Aksel, N.: Creeping films with vortices over strongly undulated bottoms. Acta Mech. **168**, 167–193 (2004).
[20] Scholle, M., Rund A., Aksel, N.: Drag reduction and improvement of material transport in creeping films. Arch. Appl. Mech. **75**, 93–112 (2006).
[21] Shetty, S., Cerro, R. L.: Flow of a thin film over a periodic surface. Int. J. Multiphase Flow **19**, 1013–1027 (1993).
[22] Trifonov, Y.: Viscous liquid film flows over a period surface. Int. J. Multiphase Flow **24**, 1139–11651 (1998).
[23] Shetty, S., Cerro, R. L.: Spreading of a liquid point source over a complex surface. Ind. Eng. Chem. Res. **37**, 626–635 (1998).
[24] Vlachogiannis, M., Bontozoglou, V.: Experiments on laminar film flow along a periodic wall. J. Fluid Mech. **457**, 133–156 (2002).
[25] Wang, C. Y.: Liquid film flowing slowly down a wavy incline. AIChE J. **27**, 207–212 (1981).

[26] Wang, C. Y.: Low Reynolds number film flow down a three-dimensional bumpy surface. ASME J. Fluid Eng. **127**, 1122–1127 (2005).
[27] Wierschem, A., Aksel, N.: Influence of inertia on eddies created in films creeping over strongly undulated substrates. Phys. Fluids **16**, 4566–4574 (2004).
[28] Wierschem, A., Aksel, N.: Hydraulic jumps and standing waves in gravity-driven flows of viscous liquids in wavy open channels. Phys. Fluids **16**, 3868–3877 (2004).
[29] Wierschem, A., Aksel, N.: Instability of a liquid film flowing down an inclined wavy plane. Physica D **186**, 221–237 (2003).
[30] Wierschem, A., Scholle, M., Aksel, N.: Creeping film flow down an inclined wavy plane. Part II. ZAMM **81**, S493–S494 (2001).
[31] Wierschem, A., Scholle, M., Aksel, N.: Vortices in film flow over strongly undulated bottom profiles at low Reynolds numbers. Phys. Fluids **15**, 426–435 (2003).
[32] Zhao L., Cerro, R. L.: Experimental characterization of viscous film flows over complex surfaces. Int. J. Multiphase Flow **18**, 495–516 (1992).

Authors' address: H. Luo and C. Pozrikidis, Department of Mechanical and Aerospace Engineering, University of California, San Diego, La Jolla, CA 92093-0411, U.S.A. (E-mail: cpozrikidis@ucsd.edu)